

# Semiclassical perspective on Landau levels and Hall conductivity in an anisotropic cubic Dirac semimetal and the peculiar case of star-shaped classical orbits

Ahmed Jellal<sup>1,2</sup>, Hocine Bahlouli<sup>3</sup>, and Michael Vogl<sup>3,4,\*</sup>

<sup>1</sup>Laboratory of Theoretical Physics, Faculty of Sciences, *Chouaib Doukkali University*, P.O. Box 20, 24000 El Jadida, Morocco

<sup>2</sup>Canadian Quantum Research Center, 204-3002 32 Avenue Vernon, British Columbia V1T 2L7, Canada

<sup>3</sup>Physics Department, *King Fahd University of Petroleum and Minerals*, Dhahran 31261, Saudi Arabia

<sup>4</sup>Interdisciplinary Research Center for Intelligent Secure Systems, *KFUPM*, Dhahran 31261, Saudi Arabia



(Received 27 April 2024; revised 11 June 2024; accepted 13 June 2024; published 26 June 2024)

We study an anisotropic cubic Dirac semimetal subjected to a constant magnetic field. In the case of an isotropic dispersion in the  $x$ - $y$  plane, with parameters  $v_x = v_y$ , it is possible to find exact Landau levels, indexed by the quantum number  $n$ , using the typical ladder operator approach. Interestingly, we find that the lowest energy level (the zero-energy state in the case of  $k_z = 0$ ) has a degeneracy that is 3 times that of other states. This degeneracy manifests in the Hall conductivity as a step at a zero chemical potential  $3/2$  the size of other steps. Moreover, as  $n \rightarrow \infty$ , we find energies  $E_n \propto n^{3/2}$ , which means the  $n$ th step as a function of the chemical potential roughly occurs at a value  $\mu \propto n^{3/2}$ . We propose that these exciting features could be used to experimentally identify cubic Dirac semimetals. Subsequently, we analyze the anisotropic case  $v_y = \lambda v_x$ , with  $\lambda \neq 1$ . First, we consider a perturbative treatment around  $\lambda \approx 1$  and find that energies  $E_n \propto n^{3/2}$  still hold as  $n \rightarrow \infty$ . To gain further insight into the Landau level structure for a maximum anisotropy, we turn to a semiclassical treatment that reveals interesting star-shaped orbits in phase space that close at infinity. This property is a manifestation of weakly localized states. Despite being infinite in length, these orbits enclose a finite phase space volume and permit finding a simple semiclassical formula for the energy, which has the same form as above. Our findings suggest that both isotropic and anisotropic cubic Dirac semimetals should leave similar experimental imprints.

DOI: [10.1103/PhysRevB.109.235434](https://doi.org/10.1103/PhysRevB.109.235434)

## I. INTRODUCTION

Semiclassical approximations are typically achieved by taking the  $\hbar \rightarrow 0$  limit of quantum mechanics [1,2]. More precisely, this is the limit at which the characteristic action  $S$  is large compared to the reduced Planck constant  $\hbar$ , that is,  $S \gg \hbar$  [3,4]. Within this limit, capturing much of quantum systems' rich and exotic behavior and preserving the intuitive explanations that classical mechanics provides are possible. More than that, semiclassical physics has allowed us to gain deep insights into the interplay between classical chaos and quantum mechanics [5]. A prototypical example of this is the effect of quantum scarring that occurs with wave functions in quantum billiards that can be traced back to the stable orbits in a corresponding classical chaotic system, where such orbits leave their imprints on the quantum wave function [6]. An even more important reason for the interest in semiclassical methods is that they provide a nonperturbative approximation scheme, which is analytically accessible—something that is exceptional.

This strength of the approach can be seen most clearly in the fact that the semiclassical method can solve problems approximately that ordinary methods such as perturbation theory cannot. For instance, if one treats the harmonic oscillator potential as a perturbation around the free particle, then perturbation theory cannot produce the well-known discrete energy levels. However, in this case, the semiclassical method is impressive because it produces exact results for the discrete energy levels [7,8].

This work does not aim to apply semiclassical methods to the ordinary Schrödinger equation with a quadratic dispersion, whose implications are well known. Instead, we want to see its consequences in the context of more exotic phases of matter—so-called semimetals.

After the discovery of graphene [9] (a single layer of carbon atoms arranged in a honeycomb pattern), researchers discovered many exciting transport properties. A famous example is Klein tunneling [10], showing that an electron under normal incidence will tunnel through a barrier with 100% probability. These features can be traced back to graphene's peculiar band structure, in which the conduction and valence bands touch at isolated points. This property made graphene an early example of a semimetal, i.e., a material in which the overlap between conduction and valence bands is not precisely zero like in an insulator or semiconductor and not of finite measure like in a conductor. Instead, while the overlap is nonzero, it has zero measure. Motivated by this discovery, much interest in similar classes of materials has emerged. One example is Dirac semimetals [11,12], which were the

\*Contact author: [ssss133@googlemail.com](mailto:ssss133@googlemail.com)

first experimentally confirmed material in this class. Dirac semimetals can be considered a three-dimensional analog of graphene [11,13] because, much like graphene, they have a linear dispersion near isolated band touching points. Dirac semimetals are interesting because the exciting linear band touching is robust. Indeed, Dirac cones do not appear due to accidental band touchings; instead, they are protected by crystalline symmetry and spin-orbit coupling [14,15] and are therefore very stable. Of course, a plethora of other kinds of semimetals with robust band features exist, such as nodal line semimetals, in which bands touch along a one-dimensional line or a more general lower-dimensional surface than the embedding space [16–18]. There are also semimetals with band touchings of higher than linear order, such as quadratic or cubic dispersion [12,19–22]. Different points in a dispersion, not just extrema, and band touching points can have interesting physical consequences for magnetic properties. For instance, it has been found that different types of saddle points can have a profound impact on magnetic breakdown [23].

In this work, we will focus our investigation on the effect of band touching points on magnetic properties in semimetals. Such effects have been studied in a variety of situations for increasingly exotic semimetals such as type II Weyl semimetals [24] and semimetals with a charge-4 touching point [25]. Our work adds to this growing literature on exotic semimetals and their magnetic properties. In particular, we will study the exotic case of an anisotropic cubic Dirac metal [12,20] subjected to a constant magnetic field. We will do so by using both fully quantum and semiclassical methods. Semiclassical results are compared to fully quantum results. Both approaches offer exciting insights and permit us to speculate about how one might experimentally identify a cubic Dirac semimetal, whether it is isotropic or anisotropic.

We organized our work as follows. In Sec. II, we introduce the Hamiltonian of the system. In Sec. III, we study the Hamiltonian for two cases that allow for an exact quantum mechanical analytical solution; these cases are isotropic in the  $x$ - $y$  plane. First, we consider the purely two-dimensional limit. Here, the material is thin, and we may restrict ourselves to momentum  $k_z = 0$  in the  $z$  direction for low energies. Next, we consider the case of  $k_z \neq 0$ , where the material is thick enough that not all momenta in the  $z$  direction are frozen out. In Sec. IV, we perturbatively consider the effect of the anisotropy by introducing a small anisotropy parameter  $\lambda \ll 1$ . In Sec. V, we recast the problem in a semiclassical language, which allows us to investigate classical orbits and study the differences between exact quantum and semiclassical results. We study the maximally anisotropic limit, which is inaccessible to a fully quantum analytical treatment. We find classical orbits and solutions for energy levels that are exact in the semiclassical limit and compare them to numerical results. Last, in Sec. VI we draw our conclusions

## II. ANISOTROPIC CUBIC DIRAC SEMIMETALS

We take the Hamiltonian describing an anisotropic cubic Dirac semimetal [12]

$$H(k) = \hbar \begin{pmatrix} h(k) & 0 \\ 0 & -h(k) \end{pmatrix} \quad (1)$$

as the starting point of our discussion. Such a Hamiltonian, for instance, is expected to be realizable in quasi-one-dimensional

molybdenum monochalcogenide compounds [12]. For such a material the basis set that was used to write the above Hamiltonian is  $|\Psi\rangle = (|A, \uparrow\rangle, |B, \uparrow\rangle, |A, \downarrow\rangle, |B, \downarrow\rangle)$ , with  $A$  and  $B$  and  $\uparrow$  and  $\downarrow$  designating the orbital and spin degrees of freedom, respectively. Of course, there is a possibility that similar Hamiltonians may be realizable in other types of materials and also with different degrees of freedom (such as sublattice degrees of freedom), giving rise to an identical matrix structure. For this reason, our results remain general in what follows, so we will not explicitly use the basis set introduced above.

The Hamiltonian (1) for our case of a cubic Dirac semimetal consists of two blocks with the form

$$h(k) = v_x(\hat{k}_+^3 + \hat{k}_-^3)\sigma_x + iv_y(\hat{k}_+^3 - \hat{k}_-^3)\sigma_y + v_z k_z \sigma_z, \quad (2)$$

where  $\hat{k}_\pm = \hat{k}_x \pm i\hat{k}_y$  are momentum operators with  $\hat{k}_i = -i\hbar\partial_i$ . Finally,  $\sigma_i$  are Pauli matrices, and  $v_{x,y,z}$  are real-valued and independent coefficients (they are not velocities) with dimension  $T^{-1}$ , where  $T$  stands for time.

A constant magnetic field  $B$  can be introduced into our description with a convenient choice of the Landau gauge. That is, it is introduced via a vector potential  $\mathbf{A} = (0, Bx, 0)$  using the minimal substitution procedure  $\mathbf{k} \rightarrow \mathbf{k} - \frac{e}{\hbar c}\mathbf{A}$ . In the unit system ( $e = c = \hbar = 1$ ), we therefore replace canonical momentum  $\hat{p}_i$  operators by kinetic momentum operators  $\hat{\pi}_i$  as

$$\hat{k}_\pm \rightarrow \hat{\pi}_\pm = \hat{k}_x \pm i(\hat{k}_y - B\hat{x}). \quad (3)$$

In the following section, we will first study this Hamiltonian's energy levels, so-called Landau levels, fully quantum mechanically, which is only possible in specific high-symmetry situations.

## III. EXACT ENERGY LEVELS FOR THE ISOTROPIC

### CASE $v_x = v_y$

#### A. Isotropic case with $k_z = 0$

The Hamiltonian describing an isotropic cubic Dirac semimetal with  $v_x = v_y = v$  and the  $z$  direction frozen out as  $k_z = 0$  (see the Appendix of [20] for a more detailed discussion of how this happens for a thin material) is given by

$$H(\hat{\mathbf{k}}, x) = 2v \begin{pmatrix} 0 & \hat{\pi}_+^3 & 0 & 0 \\ \hat{\pi}_-^3 & 0 & 0 & 0 \\ 0 & 0 & 0 & -\hat{\pi}_+^3 \\ 0 & 0 & -\hat{\pi}_-^3 & 0 \end{pmatrix}. \quad (4)$$

To solve the eigenvalue problem, we can separate variables and write the eigenspinors as plane waves in the  $y$  direction. This is due to the fact that  $[H(k), \hat{k}_y] = 0$  implies conservation of momentum along the  $y$  direction  $\Psi(x, y) = e^{ik_y y} \Psi(x)$ , with  $\Psi(x) = [\Psi_1(x), \Psi_2(x), \Psi_3(x), \Psi_4(x)]^T$ . We may now define the operators

$$\hat{a} = \frac{1}{\sqrt{2B}}[\hat{k}_x + i(k_y - B\hat{x})], \quad (5)$$

$$\hat{a}^\dagger = \frac{1}{\sqrt{2B}}[\hat{k}_x - i(k_y - B\hat{x})], \quad (6)$$

which satisfy the commutation relation  $[\hat{a}, \hat{a}^\dagger] = \mathbb{1}$  and can therefore be interpreted as ladder operators. Using this

notation, the Hamiltonian becomes

$$H = \omega_c \begin{pmatrix} 0 & \hat{a}^3 & 0 & 0 \\ \hat{a}^{\dagger 3} & 0 & 0 & 0 \\ 0 & 0 & 0 & -\hat{a}^3 \\ 0 & 0 & -\hat{a}^{\dagger 3} & 0 \end{pmatrix}, \quad (7)$$

where  $\omega_c = 2v(2eB)^{3/2}$  is called the cyclotron frequency (recall  $v$  is not velocity). The eigenvalue problem  $H(k)\Psi(x, y) = E\Psi(x, y)$  for the second spinor  $\Psi_2(x)$  component can be reduced to

$$\omega_c^2 \hat{a}^{\dagger 3} \hat{a}^3 \Psi_2(x) = E^2 \Psi_2(x), \quad (8)$$

which can be solved by harmonic oscillator states  $\Psi_2(x) = |n\rangle$ . Associated energies are given as

$$E_{n,s} = s\omega_c \sqrt{n(n-1)(n-2)}, \quad (9)$$

where  $s = \pm 1$ . Using as the ansatz  $\Psi_2(x) = |n\rangle$  in this equation, we can obtain full normalized spinors as

$$\Psi_n^{(h)}(x, y) = \frac{1}{\sqrt{2}} \begin{pmatrix} s|n-3\rangle \\ |n\rangle \\ 0 \\ 0 \end{pmatrix} e^{iky}, \quad n \geq 3, \quad (10)$$

and using a similar relation for the fourth component, we find

$$\Psi_n^{(-h)}(x, y) = \frac{1}{\sqrt{2}} \begin{pmatrix} 0 \\ 0 \\ -s|n-3\rangle \\ |n\rangle \end{pmatrix} e^{iky}, \quad n \geq 3, \quad (11)$$

Here, the label  $(h)$  stands for spinors with contributions that come solely from the upper block, and  $(-h)$  stands for the lower block in the Hamiltonian.

A special case must be considered to describe the  $n < 3$  states since they require different normalization and do not come as pairs with opposing signs. For the case  $m = 0, 1, 2$ , we find the spinors

$$\Psi_l^{(h)}(x, y) = \begin{pmatrix} 0 \\ |l\rangle \\ 0 \\ 0 \end{pmatrix} e^{iky}, \quad l < 3, \quad (12)$$

$$\Psi_l^{(-h)}(x, y) = \begin{pmatrix} 0 \\ 0 \\ 0 \\ |l\rangle \end{pmatrix} e^{iky}, \quad l < 3, \quad (13)$$

where we find that the zero-energy ground state is sixfold degenerate. This observation is interesting because it contrasts that of single-layer graphene, which has a zero-energy state with no degeneracy. This ground-state degeneracy has interesting consequences and impacts the Hall conductivity. We begin our discussion of this with the typical formula for the Hall conductivity at finite temperature

$$\sigma_{xy} = i \sum_{n,n'} [f(E^n) - f(E^{n'})] \frac{\langle \psi_n | j_x | \psi_{n'} \rangle \langle \psi_{n'} | j_y | \psi_n \rangle}{(E^n - E^{n'})^2}, \quad (14)$$

where  $|\psi_n\rangle$  is any eigenstate of the Hamiltonian,  $f(E) = \{\exp[\beta(E - \mu)] + 1\}^{-1}$  is the Fermi-Dirac distribution,  $\mu$  is the chemical potential, and  $\beta$  is the inverse temperature.

Current operators are found in the usual way by taking the derivative of the Hamiltonian with respect to a vector potential. For our eigenstates and eigenvalues, we find a unitless reduced Hall conductivity  $\sigma_{xy}^{(r)}$ , which is given as

$$\sigma_{xy}^{(r)} = \frac{h\sigma_{xy}}{4e^2} = \frac{9}{2} \omega_c^2 \sum_{n,\sigma,\sigma'} n(n-1) \frac{f(E_{n+1,\sigma}) - f(E_{n,\sigma'})}{(E_{n,\sigma'} - E_{n+1,\sigma})^2}. \quad (15)$$

Here, the sum is over  $n \in \mathbb{N}$  and  $\sigma, \sigma' \in \{-1, 1\}$ . The result of the computation can be seen in Fig. 1. It shows that the step in Hall conductivity at zero chemical potential is  $3/2$  times the step size of other steps in the quantized Hall conductivity. This result differs from the case of graphene, which we show for comparison, in which the first step is half the usual step size; for a typical Dirac semimetal, the result has the same properties as graphene. The reason for this behavior can be found in the sixfold-degenerate lowest Landau level of the cubic Dirac semimetal, which has  $3/2$  the degeneracy of other states. This property contrasts that of graphene, in which the lowest Landau level has half the degeneracy of other levels. This result also differs from a typical metal in which all steps are equally spaced. The second observation one may make is that in graphene, steps occur at a dimensionless chemical potential  $\mu^{(r)} = \sqrt{n}$ . In contrast, in the cubic Dirac semimetal case, they occur at values that asymptotically go to  $\mu^{(r)} = n^{3/2}$ . Both observations combined with the step height (it is twice that of a cubic Weyl semimetal [26]), which is due to the level degeneracy of the cubic Dirac semimetal's Landau levels, can be used to identify such materials via the quantized Hall conductivity experimentally.

### B. Quasi-two-dimensional isotropic case $k_z \neq 0$

After considering the case of a semimetal with  $k_z = 0$  (in addition to being isotropic in the  $x$ - $y$  plane), we now consider the case where the dimension of the material in the  $z$  direction is sufficiently large that considering nonzero momentum  $k_z \neq 0$  is relevant for more than just high energies. As before, we will restrict our discussion to the isotropic case. To keep our description consistent in units of the cyclotron frequency  $\omega_c$ , we define  $m = \frac{v_z k_z}{2v(\sqrt{2}B)^3}$ , which can be interpreted as a masslike term in the original Hamiltonian model (it causes a gap in the excitation spectrum). The Hamiltonian then takes the form

$$H = \omega_c \begin{pmatrix} m & \hat{a}^3 & 0 & 0 \\ \hat{a}^{\dagger 3} & -m & 0 & 0 \\ 0 & 0 & -m & -\hat{a}^3 \\ 0 & 0 & -\hat{a}^{\dagger 3} & m \end{pmatrix}. \quad (16)$$

From here, finding the Landau levels is almost immediate and follows almost the same steps as in the previous section. We find

$$E_{n,s}(m) = s\omega_c \sqrt{n(n-1)(n-2) + m^2}, \quad n \geq 3, \quad (17)$$

with  $s = \pm 1$ , where normalized eigenspinors are given as

$$\Psi_{n,s}^{(h)}(x, y) = N \begin{pmatrix} sc_n |n-3\rangle \\ |n\rangle \\ 0 \\ 0 \end{pmatrix} e^{iky}, \quad (18)$$

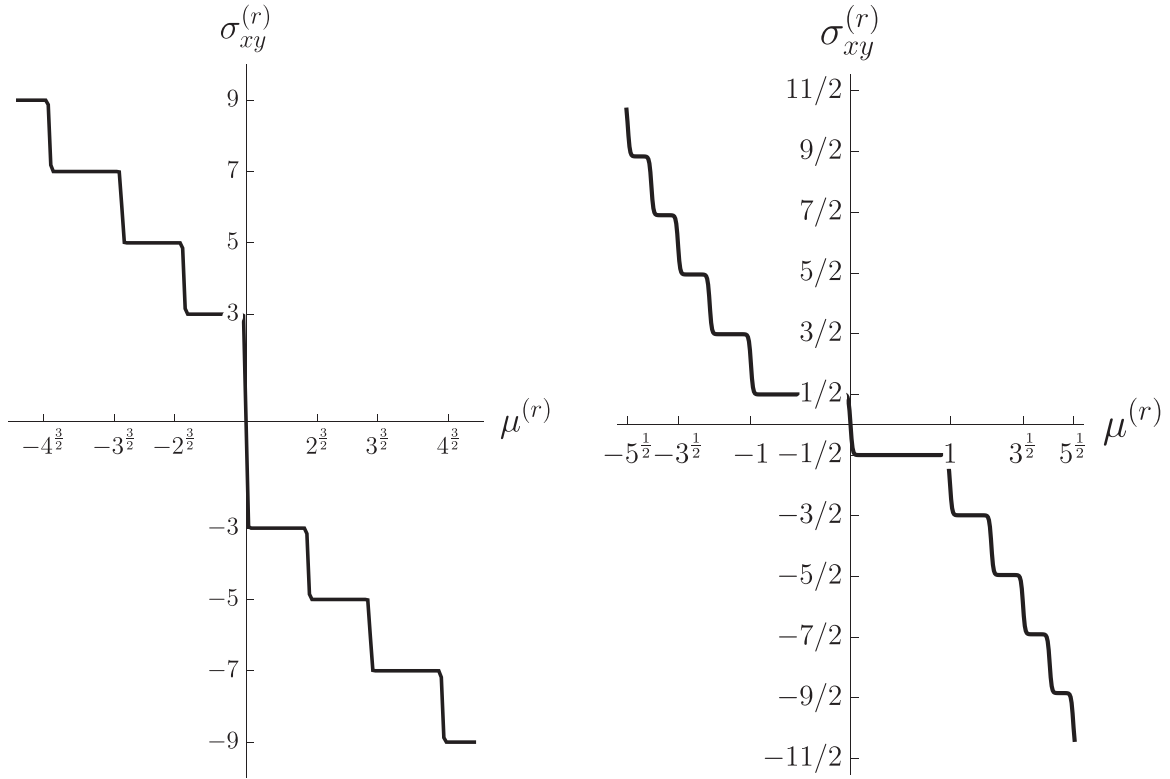


FIG. 1. Plot of the dimensionless Hall conductivity  $\sigma_{xy}^{(r)}$  as a function of dimensionless chemical potential  $\mu^{(r)} = \mu/\omega_c$ . The left panel shows the Hall conductivity for our problem of a cubic Dirac semimetal ( $\beta = 50/\omega_c$ ), and the right panel shows the case of graphene ( $\beta = 100/\omega_c$ ) as a comparison.

$$\Psi_n^{(-h)}(x, y) = N \begin{pmatrix} 0 \\ 0 \\ -sc_n |n-3\rangle \\ |n\rangle \end{pmatrix} e^{ik_y y}, \quad (19)$$

with the constants

$$c_n = \frac{E_{n,s}(0)}{E_{n,s}(m) - m}, \quad N = \frac{1}{\sqrt{c_n^2 + 1}}. \quad (20)$$

It is important to note that the case of  $n < 3$  again requires special care and has the same eigenspinors as given in Eq. (13) with corresponding eigenvalues

$$E_n^{(\pm h)} = \mp \omega_c m, \quad (21)$$

which are each threefold degenerate. It is important to stress that the  $-$  sign corresponds to the upper block of the Hamiltonian and the  $+$  sign corresponds to the lower block, which is unlike the  $n > 3$  result that has both signs in both cases. Much like the truly one-dimensional case, we can plot a Hall conductivity and get the result shown in Fig. 2.

We observe that the effect of the mass term  $m$  is that some plateaus have been broadened in width while others have been shrunk. This behavior should allow experimentalists to recognize whether electrons carry momentum in the  $z$  direction.

#### IV. PERTURBATIVE ENERGY LEVELS FOR THE CASE $v_y \neq v_x$

While it was easy to find exact energy levels in the isotropic case of  $v_y = v_x$ , this task is not simple using analytical means

for the anisotropic case of  $v_y \neq v_x$ . Introducing an anisotropy parameter  $\lambda = \frac{1-v_y/v_x}{2}$  is useful. This approach allows us to write the Hamiltonian in the convenient form

$$H = \omega_c (h_0 + \lambda h_1) \otimes \sigma_z, \quad (22)$$

with  $\lambda$  being a perturbative parameter and the definitions

$$h_0 = \begin{pmatrix} 0 & \hat{a}^3 \\ \hat{a}^{\dagger 3} & 0 \end{pmatrix}, \quad h_1 = \begin{pmatrix} 0 & \hat{a}^{\dagger 3} - \hat{a}^3 \\ \hat{a}^3 - \hat{a}^{\dagger 3} & 0 \end{pmatrix}. \quad (23)$$

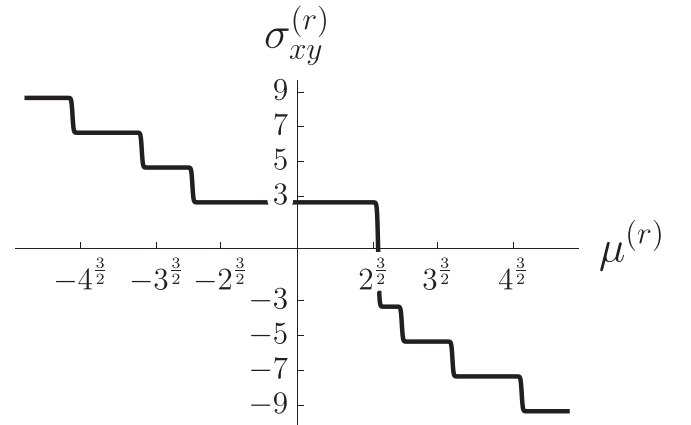


FIG. 2. Plot of the dimensionless Hall conductivity  $\sigma_{xy}^{(r)}$  as a function of the dimensionless chemical potential  $\mu^{(r)} = \mu/\omega_c$  at inverse temperature  $\beta = 50/\omega_c$ , with “mass” term  $m = -3$ .

Here,  $h_0$  corresponds to an exactly solvable isotropic Hamiltonian, and  $\lambda h_1$  is considered a perturbation. Eigenvalues  $E_n^0$  are nondegenerate in the case  $n \geq 3$ , and corrections to the energy to first order can be computed straightforwardly using the standard expressions for Rayleigh-Schrödinger perturbation theory [27] as

$$E_n = E_n^0(1 - \lambda). \quad (24)$$

Like in previous sections, the degenerate zero eigenvalue case requires special care and must be treated using degenerate perturbation theory. Interestingly, first-order degenerate perturbation theory yields no correction such that expression (24), which includes the first-order corrections to energies above, remains valid in all cases. Therefore, it is clear that a small anisotropy is not expected to have much of an impact on the qualitative picture of the Hall conductivity [to leading order  $\omega \rightarrow (1 - \lambda)\omega_c$  is the only modification].

## V. SEMICLASSICAL TREATMENT

Since a completely quantum mechanical treatment for the anisotropic case is challenging, we will resort to a semiclassical treatment in this section. This approach allows us to gain additional insights, such as the shapes of particle trajectories under the influence of a magnetic field, and further insight into the anisotropic regime, which we stress is difficult to access in a complete quantum treatment.

### A. Review of Bohr-Sommerfeld-type semiclassics for matrix Hamiltonians

A general and powerful method to determine energy levels by studying classical trajectories is the so-called Gutzwiller approach to the semiclassical density of states [1]. This approach was generalized to arbitrary matrix-valued Hamiltonians in [3]. While the method developed in [3] is quite general and allows for treatments of various special cases, our current problem of determining Landau levels for a cubic Dirac semimetal is much simpler. Notably, we have three significant simplifications:

(1) It is enough to restrict ourselves to one-dimensional Hamiltonians. We may do so because, in our case with Landau levels,  $k_y$  and  $k_z$  can be treated as parameters entering a one-dimensional (1D) Hamiltonian, that is, as complex numbers rather than *bona fide* operators.

2. The eigenvalues of the classical limit Hamiltonian  $H(p, x)$ , where the momentum operator  $\hat{p}$  was mapped to a complex number  $p$ , are nondegenerate. This simplification is possible because the  $h(k)$  blocks in Eq. (1) are not coupled; it is, therefore, enough to consider them separately, and their eigenvalues can be found to be nondegenerate.

(3) We may ignore degeneracy factors that arise from different Landau orbits over the plane. This simplification is possible because they enter only the density of states and not expressions for the energy levels that interest us.

These three simplifications mean that in what follows, we may directly employ the modified Bohr-Sommerfeld quantization condition that was derived in [3]:

$$2S_\alpha - \hbar \left[ \pi(v_\alpha + 4n) - 2 \int_0^{T_\alpha} dt M_\alpha \right] = 0. \quad (25)$$

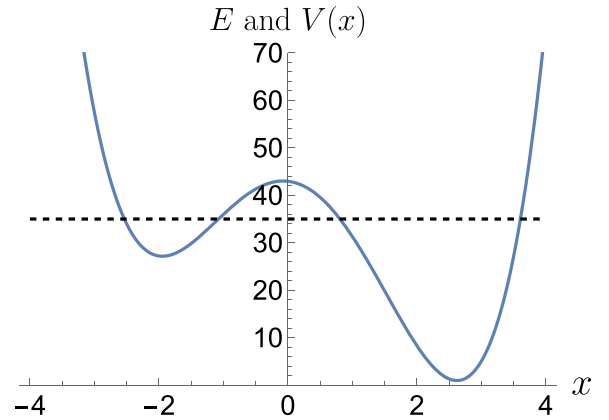


FIG. 3. Plot of the potential landscape  $V(x)$  (thick blue line) and energy (dashed line). Two distinct potential pots are visible. Each will have its own associated classical periodic orbits with an action  $S_\alpha$ .

In what follows, we will choose units with  $\hbar = 1$ . We now move on to explain the different terms that enter this expression. Here,  $n$  is an integer that will label energy levels,  $S_\alpha$  is the classical action, and  $T_\alpha$  is the time it takes to traverse a primitive periodic orbit, an orbit in phase space that has been traversed only once. The index  $\alpha$  accounts for different periodic orbits being possible at a fixed energy. There are two ways this can happen.

(1) Potentials can allow for different periodic orbits at a given energy  $E$  like in Fig. 3.

(2) We deal with matrix Hamiltonians. That is, to the lowest order, the Schrödinger equation is replaced by a simple matrix equation

$$H(x, p_x = \partial_x S)V = EV. \quad (26)$$

For an  $N \times N$  Hamiltonian this can be diagonalized to determine  $N$  eigenvectors  $V_i$  and  $N$  eigenvalue equations that determine actions  $S_\alpha$ ,

$$H_i(x, p_x = \partial_x S_\alpha) = E, \quad (27)$$

which are ordinary Hamilton-Jacobi equations, where  $H_i$  are eigenvalues of  $H(x, \partial_x S)$ . These Hamilton-Jacobi equations can have one or more periodic orbits associated with a given energy  $E$ .

Next, in our expression, Eq. (25) enters  $v_\alpha$ , which is the so-called Maslov index which for 1D motion counts the number of reflections by a potential barrier (or, more generally, directional changes) that a particle experiences while it traverses a periodic orbit. The last term that enters is the so-called semiclassical phase factor

$$M_\alpha = \text{Im}\{V_\alpha^\dagger [\partial_{p_x} H(x, p_x)] \partial_x V_\alpha\}, \quad (28)$$

which bears some resemblance to a Berry phase, as discussed in [3, 28–31]. Here,  $V_\alpha$  is the eigenvector of the classical Hamiltonian matrix  $H(x, \partial_x S_\alpha)$  corresponding to the orbit  $\alpha$ .

### B. The Hamiltonian system

For our computations of semiclassical energies, we will consider only the upper block of (1), that is, Eq. (2) with the

magnetic field introduced as before via minimal substitution. This simplification is possible because the second block in Eq. (1) will yield (up to a sign) the same energies as the other block. The semiclassical limit of the Hamiltonian (2) is then obtained by replacing momentum operators with canonical momenta  $\hat{p}_i \rightarrow \partial_{x_i} S = p_i$ . We obtain the classical expression

$$h(\pi_i) = 2v_x \begin{pmatrix} 0 & \pi_+^3 + \lambda(\pi_-^3 - \pi_+^3) \\ \pi_-^3 + \lambda(\pi_+^3 - \pi_-^3) & 0 \end{pmatrix}, \quad (29)$$

and we introduce the shorthand notations

$$\pi_{\pm} = p_x \pm i(p_y + eBx), \quad (30)$$

where  $p_i$  are canonical momenta and  $\pi_i$  are kinetic momenta. The parameter  $\lambda = \frac{1-v_y/v_x}{2}$  measures the degree of anisotropy, as discussed previously.

### C. Isotropic two-dimensional case $k_z, \lambda = 0$

In the isotropic case, we may set  $\lambda = 0$  and  $v_x = v_y = v$ ; for a thin sheet, low energies correspond to  $k_z = 0$ , and we find

$$h(\pi) = 2v \begin{pmatrix} 0 & \pi_+^3 \\ \pi_-^3 & 0 \end{pmatrix}. \quad (31)$$

The eigenvalues are obtained from the determinant as  $\det[h(\pi_i) - E] = 0$ ,

$$E_s = 2sv\sqrt{(\pi_+\pi_-)^3}, \quad (32)$$

where  $s = \pm 1$ . The corresponding normalized eigenvectors are given by

$$V = \frac{1}{\sqrt{2}} \begin{pmatrix} \frac{2v}{E_s} \pi_+^3 \\ 1 \end{pmatrix}. \quad (33)$$

At this level, we see that there are two classical Hamiltonians of the form

$$H(p_i, x) = 2sv[p_x^2 + (p_y + eBx)^2]^{3/2}. \quad (34)$$

#### 1. Time for an orbit

Another ingredient that enters our expression for the generalized Bohr-Sommerfeld quantization condition is the time for an orbit. Here, we start by investigating the equations of motion, which are given by Hamilton's equations

$$\dot{q} = \frac{\partial H}{\partial p}, \quad \dot{p} = -\frac{\partial H}{\partial q}, \quad (35)$$

where  $q$  is the position and  $p$  is momentum coordinates. In our case, we find

$$\begin{aligned} \dot{x} &= 3s(4|E|v^2)^{\frac{1}{3}} p_x, \\ \dot{y} &= 3s(4|E|v^2)^{\frac{1}{3}} (p_y + eBx), \\ \dot{p}_x &= 3seB(4|E|v^2)^{\frac{1}{3}} (p_y + eBx), \\ \dot{p}_y &= 0. \end{aligned} \quad (36)$$

From (36) we find (taking a time derivative of  $\dot{x}$  and using the equation for  $\dot{p}_x$ ) that the equation of motion for the  $x$  coordinate is given as

$$\ddot{x} = -\omega^2(x + x_s), \quad (37)$$

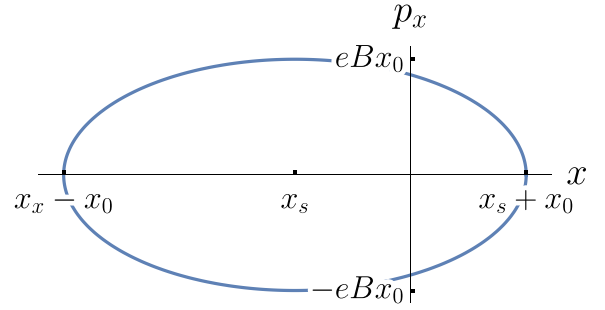


FIG. 4. Phase space curve of an electron in a cubic semimetal subjected to a constant magnetic field.

which constitutes a shifted harmonic oscillator with position shift  $x_s = p_y/(eB)$  (note that  $p_y$  is constant, as shown above). It is important to note that this equation is valid for both classical Hamiltonians in Eq. (34). It also means that it is enough to consider only one of the eigenvalues to find semiclassical energy levels. Indeed, in the remainder of this section, we will focus on only one of the Hamiltonians and therefore drop all indices related to orbits. The oscillator frequency is found to be

$$\omega = 3(4|E|v^2)^{\frac{1}{3}} eB. \quad (38)$$

The time for an orbit as per the definition  $\omega = 2\pi/T$  then is then found to be

$$T = \frac{2\pi}{3(4|E|v^2)^{\frac{1}{3}} eB}. \quad (39)$$

#### 2. Classical orbit, action, and the Maslov index

Now, from Eq. (37), we find the solutions

$$x = x_s + x_0 \sin(\omega t), \quad p_x = seBx_0 \cos(\omega t), \quad (40)$$

with amplitude

$$x_0 = \frac{1}{eB} \left( \frac{|E|}{2v} \right)^{\frac{1}{3}}, \quad (41)$$

which can be found for a given energy by placing the solutions (40) in Eq. (32). Plotting them, we get the typical phase space curve of a harmonic oscillator that can be seen in Fig. 4, which is just an elliptic orbit. This curve directly tells us that the particle along each orbit changes direction twice, and therefore, the Maslov index is

$$\nu_\alpha = 2. \quad (42)$$

We may next use  $p_x = \partial_x S$  in Eq. (32) to find the action for an orbit as

$$S = \int \sqrt{\left( \frac{|E|}{2v} \right)^{\frac{2}{3}} - (p_y + eBx)^2} dx. \quad (43)$$

This integral for a single period of a primitive orbit gives

$$S = \frac{\pi}{eB} \left( \frac{|E|}{2v} \right)^{\frac{2}{3}}. \quad (44)$$

### 3. Semiclassical Berry-like phase and energy levels

For the semiclassical phase term using (28) we find

$$M_{\pm} = 9eB \left( \frac{|E|v^2}{2} \right)^{\frac{1}{3}}, \quad (45)$$

which is a constant, and therefore, the integral  $\int_0^T dt M = MT = 3\pi$  is trivial.

We may use our results (44), (42), and (45) and put them into (25) to find that our semiclassical energies are then given by

$$E = \pm \omega_c (n-1)^{3/2}, \quad (46)$$

with  $\omega_c = 2v(2eB)^{3/2}$ .

### 4. Performance of semiclassical results

Understanding under what conditions the semiclassical results perform well compared to the exact results obtained earlier is helpful. Of course, we see directly that the results are different. This observation poses the question of under which conditions the results agree.

Typically, semiclassical results are reliable for large quantum numbers. Therefore, we do an expansion for large  $n$  of both the exact ( $E_{\text{exact}}$ ) and semiclassical ( $E_{\text{semcl}}$ ) results to find

$$\begin{aligned} E_{\text{exact}} &= \pm \omega_c \left( n^{3/2} - \frac{3}{2}n^{1/2} + \frac{3}{8}n^{-1/2} \right) + O(n^{-3/2}), \\ E_{\text{semcl}} &= \pm \omega_c \left( n^{3/2} - \frac{3}{2}n^{1/2} - \frac{1}{8}n^{-1/2} \right) + O(n^{-3/2}), \end{aligned} \quad (47)$$

where we can see that results agree well in the limit of large quantum numbers—they only disagree at order  $O(n^{-1/2})$ , which is typical in the semiclassical approach—because, typically, larger quantum numbers correspond to a larger classical action.

### D. Quasi-two-dimensional isotropic limit

Next, we consider the case  $p_z \neq 0$ , which can describe a sheet of finite thickness. To obtain a simpler notation that we can compare to the exact quantum case, we set  $p_z = m\omega_c/(2v_z)$ . The notation is suggestive and clarifies that  $p_z$  takes the role of a mass term  $m$ . The Hamiltonian then takes the form

$$h(\pi) = 2v \begin{pmatrix} \frac{m\omega_c}{2v} & \pi_+^3 \\ \pi_-^3 & -\frac{m\omega_c}{2v} \end{pmatrix}. \quad (48)$$

The eigenvalues are readily found as

$$E = 2vs \sqrt{(\pi_+ \pi_-)^3 + \left( \frac{m\omega_c}{2v} \right)^2}, \quad (49)$$

with  $s$  being the sign of the energy. The corresponding eigenvectors can be written as

$$V = \sqrt{2} \sqrt{1 - \frac{m\omega_c}{E}} \begin{pmatrix} \frac{\pi_+^3 v}{E - 2m\omega_c} \\ 1 \end{pmatrix}. \quad (50)$$

The classical system will reduce to a harmonic oscillator if we use the same methods as in the previous section. However,

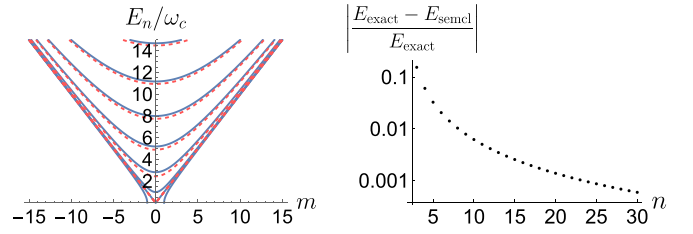


FIG. 5. The left plot shows Landau levels as a function of the mass parameter  $m$  (a dimensionless version of momentum  $k_z$ ). The right plot shows the relative error between the exact and approximate energies for  $m = 0$ .

this time it has a slightly modified driving frequency

$$\omega = 3 \left( \frac{2v(|E|^2 - m^2\omega_c^2)}{|E|^{3/2}} \right)^{\frac{2}{3}} eB. \quad (51)$$

Considering the limit of small mass and the relation to the frequency in the massless case, Eq. (38) is interesting. We will use the term  $\omega_0$  to refer to the frequency of the massless case below. In the limit of small masses, the oscillation frequency becomes

$$\omega \approx \omega_0 - \frac{2}{3} \frac{m^2 \omega_c^2}{|E|^2} \omega_0, \quad (52)$$

which tells us that a mass term reduces the oscillation frequency just as intuition would dictate. Because we have harmonic motion, we find a Maslov index

$$\nu = 2. \quad (53)$$

The action of a primitive can be computed in analogy to the previous case and is given as

$$S = \frac{\pi(|E|^2 - m^2\omega_c^2)^{\frac{1}{3}}}{2^{2/3} eB v^{2/3}}. \quad (54)$$

Last, we find that the semiclassical phase factor has the form

$$M = \frac{9Be[v(|E|^2 - 4m^2\omega_c^2/v^2)]^{2/3}}{2^{1/3} E}, \quad (55)$$

which is a constant. Therefore, the integral  $\int_0^T dt M = 2\pi M/\omega = 3\pi$  is trivial.

Applying the Bohr-Sommerfeld quantization condition (25) as before, we find that energy levels are given as

$$E_{\text{semcl}} = \omega_c \sqrt{m^2 + (n-1)^3}. \quad (56)$$

We may now compare the semiclassical result  $E_{\text{semcl}}$  to the exact result (17), which we denote  $E_{\text{exact}}$ , to find

$$E_{\text{semcl}} - E_{\text{exact}} = (n-1) \frac{\omega_c}{2m} + O(m^{-3}), \quad (57)$$

which tells us that, similar to expectations, a mass term turns the energy levels more classical (the approximation error shrinks for large mass).

To better visualize how accurate the approximation is in various situations, we plot the Landau levels as a function of the mass parameter  $m$ . The approximation's effectiveness for the worst case of  $m = 0$  is also visualized in Fig. 5. We find that the semiclassical energy levels agree very well with

exact results except for the lowest energy. The agreement improves as the “mass” is increased, which mirrors the typical quantum intuition that semiclassical approximations work especially well for massive objects. Furthermore, as expected, the approximation error decreases rapidly as a function of the quantum number  $n$ , even in the least well approximated case of  $m = 0$ .

### E. Maximally anisotropic case $v_x = 0$

In the last part of this section, we consider a case that is difficult to solve by analytical means in an exact quantum treatment: the case of a maximally anisotropic cubic Dirac semimetal. Maximum anisotropy is achieved for  $v_x = 0$  and  $v_y = v$ , where the classical Hamiltonian takes the form

$$H = v \begin{pmatrix} 0 & \pi_-^3 - \pi_+^3 \\ \pi_+^3 - \pi_-^3 & 0 \end{pmatrix}. \quad (58)$$

For this case, it is advantageous to combine Hamilton-Jacobi equations for different eigenvalues into a single Hamilton-Jacobi equation  $\det(E - H) = 0$ , and we find

$$E^2 + v^2(\pi_-^3 - \pi_+^3)^2 = 0. \quad (59)$$

Eigenvectors that correspond to different solutions for  $E$  are given as

$$V_{\pm} = \frac{1}{\sqrt{2}} \begin{pmatrix} \pm 1 \\ 1 \end{pmatrix} \quad (60)$$

and are independent of momenta and positions, which directly lets one realize that the semiclassical phase  $M$  will have no contributions. It is, therefore, important to recognize that the main contribution to orbits will be from the classical phase space orbit. The combined Hamilton-Jacobi equation (59) can be interpreted as an implicit relation for the orbit in phase space

$$E^2 - 4v^2(Bex + p_y)^2 [(Bex + p_y)^2 - 3p_x^2]^2 = 0, \quad (61)$$

which leads to the interesting phase space orbit shown in Fig. 6.

We observe that semiclassical particles in this problem traverse star-shaped orbits in phase space. These orbits do not close except at infinity (for a nonzero value of  $v_x$ , the closure happens at a finite value, however). It is clear from Fig. 6 that despite orbits that close only at infinity, the phase space volume enclosed by the trajectory is finite. This observation is interesting and peculiar because the finite phase space volume implies discretized energy levels corresponding to localized states. At the same time, the classical particles are not localized: they move to infinity along the sides of the star. This observation demonstrates how a particle can be localized for a quantum mechanical problem. The classical dynamics do not reflect this in the real space trajectory, only in phase space through a finite volume. The Maslov index can also easily be found from Fig. 6 if we note that barrier reflections happen when the momentum derivative becomes infinite; this happens at four spots along the orbit (the two spikes at  $\tilde{x} = 0$  and the indents at  $\tilde{p}_x = 0$ ). Therefore, the Maslov index in Eq. (25) is  $\nu = 4$ .

The last ingredient in Eq. (25) to find semiclassical energies is the action, which is the volume enclosed by the orbit.

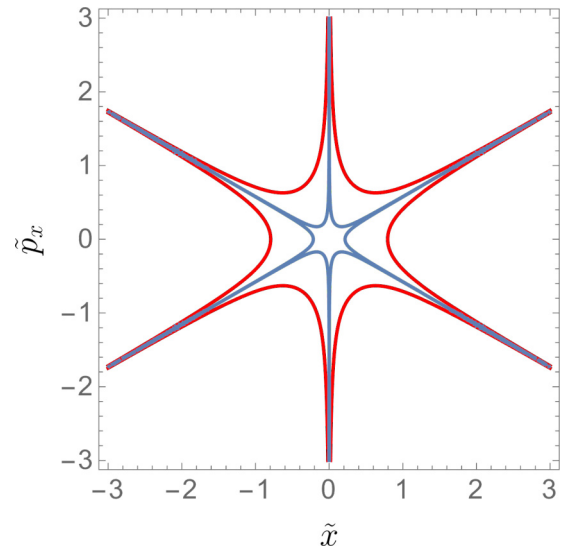


FIG. 6. Plot of phase space trajectories in terms of unitless momentum  $\tilde{p}_i = p_i(eB)^{-1/2}$ , unitless energy  $\epsilon = Ev^{-1}(eB)^{-3/2}$ , and position  $\tilde{x} = x(eB)^{1/2}$  (recall that  $v$  is not a velocity and we set  $\hbar = 1$ ). In both cases, we set  $p_y = 0$  because this term leads to only a shift of the trajectory center along the  $x$  axis. The red curve is for  $\epsilon = 1$ , and the blue one is for  $\epsilon = 0.02$ .

The simplest way to do this is to realize that it is enough to compute the area of one of the four star sectors, which is marked in blue Fig. 7. We find that the area can be separated into different pieces, giving a *unitless action*  $s$  with

$$s/4 = \int_0^\infty dx \sqrt{\frac{2x^3 + \epsilon}{6x}} - \int_{\epsilon^{1/3} 2^{-1/3}}^\infty dx \sqrt{\frac{2x^3 - \epsilon}{6x}}. \quad (62)$$

The integral simplifies considerably to

$$s = \frac{2^{4/3} \sqrt{\pi} \epsilon^{2/3} \Gamma(\frac{7}{6})}{\Gamma(\frac{5}{3})}, \quad (63)$$

where  $\Gamma$  is the gamma function. After units are reintroduced, the result is inserted into the Bohr-Sommerfeld quantization condition, and the resulting relation is solved for the energy.

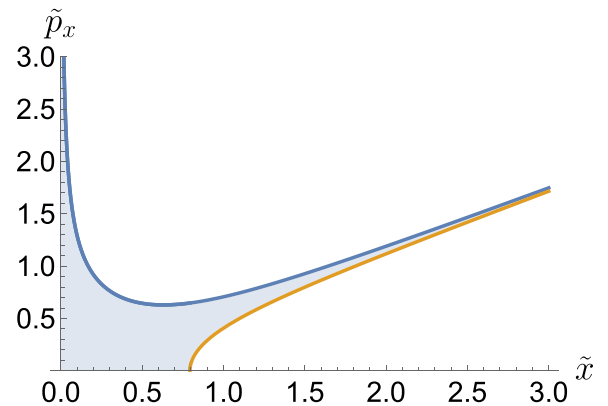


FIG. 7. Plot of one sector of the star orbit. Marked in blue is the area one needs to compute. The blue curve is given by  $\tilde{p}_x = \sqrt{x^2/3 + \epsilon/(6x)}$ , and the orange curve is given by  $\tilde{p}_x = \sqrt{x^2/3 - \epsilon/(6x)}$ .

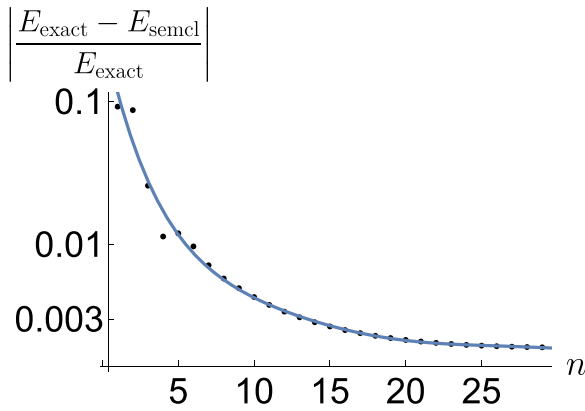


FIG. 8. The relative error between exact and approximate energies. The blue line serves to guide the eye.

We find the semiclassical energy levels are given by

$$E_n = \hbar\omega_c \frac{\pi^{3/4} \Gamma(\frac{5}{3})^{3/2}}{8\Gamma(\frac{7}{6})^{3/2}} n^{3/2}, \quad (64)$$

which, much like in the isotropic case, behave as  $E_n \propto n^{3/2}$ , but with a different proportionality constant. Of course, it is interesting that we obtained relatively simple closed-form results semiclassically in a case for which a full quantum treatment is difficult. Even a proper numerical treatment is numerically expensive because particles are only weakly localized (for details, see the Appendix). We compare our closed-form semiclassical approximation to the numerical results in Fig. 8 to determine whether our approximation is reliable. One can observe that the results are in excellent agreement with a complete numerical treatment and that the quality of agreement improves for an increasing quantum number  $n$ . The existence of discrete energy levels demonstrates that the classically nonlocalized particles are weakly quantum localized. Moreover, the functional form of the energies tells us that even in an anisotropic case, one can expect behavior for the Hall conductivity similar to what we have predicted for the isotropic case.

## VI. CONCLUSION

In summary, we showed that the Landau levels of a cubic Dirac semimetal exhibit intriguing features both quantum mechanically and from a classical perspective. We showed in a fully quantum mechanical treatment that one can expect experimentally detectable signatures of a cubic Dirac semimetal in the Hall conductivity, and we found explicit analytical expressions. While the anisotropic case could not be understood by employing a full quantum treatment, we made much more progress on the semiclassical side.

Interestingly, we found that in the anisotropic case, the electrons do not localize classically. Instead, they move infinitely far from the origin. However, they were found to

be quantum mechanically weakly localized, giving rise to discrete energy levels. Our work also provides an exciting example of quantum corrections playing a significant role in localization, enriching the phenomenological literature in this respect. Nevertheless, weak localization from the classical side has left its imprint in that the numerics for finding exact quantum energy levels are relatively expensive when using a local set of basis functions.

The PYTHON code employing sparse matrix diagonalization is available from the authors upon reasonable request.

## ACKNOWLEDGMENTS

The authors gratefully acknowledge the support provided by the Deanship of Research Oversight and Coordination (DROC) at King Fahd University of Petroleum and Minerals (KFUPM) for funding this work through Exploratory Research Grant No. ER221002.

## APPENDIX: NUMERICAL SOLUTION OF THE MAXIMALLY ANISOTROPIC CASE

For a numerical treatment, we express the Hamiltonian (58) in terms of the usual Landau basis as

$$h = \frac{\omega_c}{2} \begin{pmatrix} 0 & a^{\dagger 3} - a^3 \\ a^3 - a^{\dagger 3} & 0 \end{pmatrix}, \quad (A1)$$

and we use the fact that we may write

$$(a^3)_{ij} = \sqrt{2i + 3i^2 + i^3} \delta_{i+3,j}. \quad (A2)$$

A naive expansion letting  $i$  and  $j$  run from zero to a cutoff does not yield valid results. Indeed, as one can already check in the isotropic case, such an approach leads to issues with unphysical states at zero energy. One finds a sixfold degeneracy instead of the actual physical threefold degeneracy. Luckily, there is a simple way to fix this if one replaces

$$a^3 \rightarrow (a^3)_{\text{chop},x,y}, \quad (A3)$$

where  $(a^3)_{c,x}$  has the last three columns chopped from the matrix and  $(a^3)_{c,y}$  has the last three rows chopped. In the isotropic case, this replacement leads to the correct number of zero modes and the correct eigenvectors for the zero modes, which justifies this replacement.

For the anisotropic case, we may then write the numerical Hamiltonian as

$$h_{\text{chop}} = \frac{\omega_c}{2} \begin{pmatrix} 0 & (a^{\dagger 3})_{c,x} - (a^3)_{c,x} \\ (a^3)_{c,x} - (a^{\dagger 3})_{c,y} & 0 \end{pmatrix}, \quad (A4)$$

which leads to the results employed in the main text. We should also note that this approach is slowly converging, so a basis of  $\sim 2^{22}$  states was needed (close to state-of-the-art system sizes in exact diagonalization) to generate the results in the main text.

[1] M. C. Gutzwiller, Periodic orbits and classical quantization conditions, *J. Math. Phys.* **12**, 343 (1971).

[2] H. A. Kramers, Wellenmechanik und halbzahlige quantisierung, *Z. Phys.* **39**, 828 (1926).

- [3] M. Vogl, O. Pankratov, and S. Shallcross, Semiclassics for matrix hamiltonians: The Gutzwiller trace formula with applications to graphene-type systems, *Phys. Rev. B* **96**, 035442 (2017).
- [4] B. A. Loewe Yanez, Bridges between quantum and classical mechanics: Directed polymers, flocking and transitionless quantum driving, Ph.D. thesis, Georgia Institute of Technology, 2017.
- [5] P. Cvitanović, R. Artuso, R. Mainieri, G. Tanner, and G. Vattay, *Chaos: Classical and Quantum* (Niels Bohr Institute, Copenhagen, 2016).
- [6] E. J. Heller, Bound-state eigenfunctions of classically chaotic Hamiltonian systems: Scars of periodic orbits, *Phys. Rev. Lett.* **53**, 1515 (1984).
- [7] H. Kleinert, Semiclassical time evolution amplitude, in *Path Integrals in Quantum Mechanics, Statistics, Polymer Physics, and Financial Markets* (World Scientific, Singapore), pp. 369–457.
- [8] E. J. Saletan and A. H. Cromer, *Theoretical Mechanics* (John Wiley & Sons, 1971).
- [9] K. S. Novoselov, A. K. Geim, S. V. Morozov, D. Jiang, Y. Zhang, S. V. Dubonos, I. V. Grigorieva, and A. A. Firsov, Electric field effect in atomically thin carbon films, *Science* **306**, 666 (2004).
- [10] M. I. Katsnelson, K. S. Novoselov, and A. K. Geim, Chiral tunnelling and the Klein paradox in graphene, *Nat. Phys.* **2**, 620 (2006).
- [11] Z. Liu *et al.*, Discovery of a three-dimensional topological Dirac semimetal,  $\text{Na}_3\text{Bi}$ , *Science* **343**, 864 (2014).
- [12] Q. Liu and A. Zunger, Predicted realization of cubic Dirac fermion in quasi-one-dimensional transition-metal monochalcogenides, *Phys. Rev. X* **7**, 021019 (2017).
- [13] Z. K. Liu, J. Jiang, B. Zhou, Z. J. Wang, Y. Zhang, H. M. Weng, D. Prabhakaran, S.-K. Mo, H. Peng, P. Dudin, T. Kim, M. Hoesch, Z. Fang, X. Dai, Z. X. Shen, D. L. Feng, Z. Hussain, and Y. L. Chen, A stable three-dimensional topological Dirac semimetal  $\text{Cd}_3\text{As}_2$ , *Nat. Mater.* **13**, 677 (2014).
- [14] S. K. Kushwaha *et al.*, Bulk crystal growth and electronic characterization of the 3D Dirac semimetal  $\text{Na}_3\text{Bi}$ , *APL Mater.* **3**, 041504 (2015).
- [15] J. W. Han, S.-W. Kim, W. S. Kyung, C. Kim, G. Cao, X. Chen, S. D. Wilson, S. Cheon, and J. S. Lee, Nonsymmorphic Dirac semimetal and carrier dynamics in the doped spin-orbit-coupled Mott insulator  $\text{Sr}_2\text{IrO}_4$ , *Phys. Rev. B* **102**, 041108(R) (2020).
- [16] C. Fang, H. Weng, X. Dai, and Z. Fang, Topological nodal line semimetals, *Chin. Phys. B* **25**, 117106 (2016).
- [17] R. Yu, Z. Fang, X. Dai, and H. Weng, Topological nodal line semimetals predicted from first-principles calculations, *Front. Phys.* **12**, 127202 (2017).
- [18] H. Rostami, E. Cappelluti, and A. V. Balatsky, Helical metals and insulators: Sheet singularity of the inflated Berry monopole, *Phys. Rev. B* **98**, 245114 (2018).
- [19] C. Fang, M. J. Gilbert, X. Dai, and B. A. Bernevig, Multi-Weyl topological semimetals stabilized by point group symmetry, *Phys. Rev. Lett.* **108**, 266802 (2012).
- [20] A. Bouhlal, A. Jellal, H. Bahlouli, and M. Vogl, Tunneling in an anisotropic cubic Dirac semi-metal, *Ann. Phys. (NY)* **432**, 168563 (2021).
- [21] A. Bouhlal, A. Abbout, A. Jellal, H. Bahlouli, and M. Vogl, Tunneling phase diagrams in anisotropic multi-Weyl semimetals, *Ann. Phys. (Berlin, Ger.)* **534**, 2200267 (2022).
- [22] Y. J. Jin, Y. Xu, Z. J. Chen, and H. Xu, Type-II quadratic and cubic Weyl fermions, *Phys. Rev. B* **105**, 035141 (2022).
- [23] V. A. Zakharov, A. M. Bozkurt, A. R. Akhmerov, and D. O. Oriekhov, Landau quantization near generalized Van Hove singularities: Magnetic breakdown and orbit networks, *Phys. Rev. B* **109**, L081103 (2024).
- [24] Z.-M. Yu, Y. Yao, and S. A. Yang, Predicted unusual magnetoresistance in type-II Weyl semimetals, *Phys. Rev. Lett.* **117**, 077202 (2016).
- [25] C. Cui, X.-P. Li, D.-S. Ma, Z.-M. Yu, and Y. Yao, Charge-four Weyl point: Minimum lattice model and chirality-dependent properties, *Phys. Rev. B* **104**, 075115 (2021).
- [26] Y. Barlas, K. Yang, and A. H. MacDonald, Quantum Hall effects in graphene-based two-dimensional electron systems, *Nanotechnology* **23**, 052001 (2012).
- [27] E. Schrödinger, Quantisierung als eigenwertproblem, *Ann. Phys. (Berlin, Ger.)* **385**, 437 (1926).
- [28] P. Carmier and D. Ullmo, Berry phase in graphene: Semiclassical perspective, *Phys. Rev. B* **77**, 245413 (2008).
- [29] S. Keppeler, Semiclassical quantisation rules for the Dirac and Pauli equations, *Ann. Phys. (NY)* **304**, 40 (2003).
- [30] J. Bolte and S. Keppeler, A semiclassical approach to the Dirac equation, *Ann. Phys. (NY)* **274**, 125 (1999).
- [31] J. Bolte and S. Keppeler, Semiclassical time evolution and trace formula for relativistic spin-1/2 particles, *Phys. Rev. Lett.* **81**, 1987 (1998).